Letter | Editors' Suggestion

Mesoscopic fluctuations and multifractality at and across measurement-induced phase transitions

Igor Poboiko, Igor V. Gornyi, and Alexander D. Mirlin
Institute for Quantum Materials and Technologies, Karlsruhe Institute of Technology, 76131 Karlsruhe, Germany
and Institut für Theorie der Kondensierten Materie, Karlsruhe Institute of Technology, 76131 Karlsruhe, Germany

(Received 15 July 2025; revised 25 August 2025; accepted 1 December 2025; published 19 December 2025)

We explore statistical fluctuations over the ensemble of quantum trajectories in a model of two-dimensional free fermions subject to projective monitoring of local charge across the measurement-induced phase transition. Our observables are the particle-number covariance between spatially separated regions, G_{AB}, and the two-point density correlation function, $\mathcal{C}(r)$. Our results exhibit a remarkable analogy to Anderson localization, with G_{AB} corresponding to two-terminal conductance and $\mathcal{C}(r)$ to two-point conductance, albeit with different replica limits and unconventional symmetry class, geometry, and boundary conditions. In the delocalized phase, G_{AB} exhibits "universal," nearly Gaussian, fluctuations with variance of order unity. In the localized phase, we find a broad distribution of G_{AB} with $\overline{-\ln G_{AB}} \sim L$ (where L is the system size) and the variance $\mathrm{var}(\ln G_{AB}) \sim L^{\mu}$, and similarly for $\mathcal{C}(r)$, with $\mu \approx 0.5$. At the transition point, the distribution function of G_{AB} becomes scale invariant and $\mathcal{C}(r)$ exhibits multifractal statistics, $\overline{\mathcal{C}^q(r)} \sim r^{-q(d+1)-\Delta_q}$. We characterize the spectrum of multifractal dimensions Δ_q. Our findings lay the groundwork for mesoscopic theory of monitored systems, paving the way for various extensions.

DOI: 10.1103/2k3q-h6lz

Introduction. Many-body quantum systems subjected to quantum measurement exhibit remarkably rich physics. A peculiar property of quantum measurements is the nonunitary character of the associated dynamics of the quantum state, involving its collapse (strong or weak, depending on the measurement strength). The problem of the dynamics of a system under multiple measurements taking place randomly in space and time has been the subject of intense research in recent years. It was found that the competition between unitary dynamics and quantum measurements may result in transitions between phases with different scaling of the entanglement entropy S (which is a measure of quantum information) with the size ℓ of a subsystem [1–7] (see also reviews [8,9] and Refs. [10–13] for experimental studies). Specifically, for frequent measurements, S scales as the area of the subsystem boundary $\sim \ell^{d-1}$. In such an area-law phase, the entanglement is localized in the boundary region. When the measurement rate is lowered, the system may undergo a transition into a phase with a faster increase of $S(\ell)$, implying a delocalization of quantum information.

Many-body systems of free fermions, with local monitoring preserving Gaussianity of the quantum state [4,14–25], exhibit distinct physics. Specifically, it was found that, for $d = 1$ complex fermions, the system is asymptotically ($L \to \infty$) in the area-law phase for any nonzero monitoring rate [20,25]. For higher spatial dimensionality, $d > 1$, the system exhibits a transition between the area-law ("localized") phase and a "diffusive" phase with $\ell^{d-1} \ln \ell$ scaling of $S(\ell)$ [21,22]. These results are obtained analytically by mapping to a replica nonlinear sigma model, with its subsequent renormalization-group analysis, and supported by numerical simulations. This field theory demonstrates a remarkable analogy between the measurement-induced phase transition (MIPT) in d dimensions and Anderson localization transition in $d + 1$ dimensions, albeit with important differences in the replica limit and the symmetry class.

The dynamical evolution of a monitored system is characterized by a "quantum trajectory" determined by the outcomes of all measurements, which are stochastic due to the nature of quantum measurements. Thus, the entanglement entropy or any other property of the system will, in fact, depend on a specific quantum trajectory. Most of the analytic and numerical studies deal with averaged observables—which is, in particular, sufficient to observe the phase transition. At the same time, fluctuations of observables over the ensemble of quantum trajectories are also of great interest. We will term these fluctuations "mesoscopic," in view of the above link to Anderson localization, where mesoscopic fluctuations are those over the ensemble of disorder realizations. While fluctuations of some quantities appeared in several previous works on monitored systems (see, e.g., Refs. [14,22,26–32]), their numerical and analytical investigations are still largely in their infancy.

In this Letter, we explore mesoscopic fluctuations of key observables across the MIPT in a free-fermion system. For the numerical study, we use the $d = 2$ model, in which the transition was established in Ref. [21]. It was found there that the particle-number covariance G_{AB} plays a role of the scaling variable akin to the dimensionless conductance. Here, we

show that G_{AB} exhibits "universal conductance fluctuations" in the delocalized phase and another type of universality in the localized phase, where a broad distribution with the average $\overline{-\ln G_{AB}} \sim L$ and the variance $\mathrm{var}(\ln G_{AB}) \sim L^{\mu}$, with $\mu \approx 0.5$, sets in. The transition point is characterized by a scale-invariant distribution of G_{AB}. Furthermore, we study fluctuations of the density correlation function $\mathcal{C}(r)$ (a counterpart of two-point conductance). In particular, we show that the critical point is characterized by multifractal statistics, $\overline{\mathcal{C}^q(r)} \sim r^{-q(d+1)-\Delta_q}$, and determine the spectrum of multifractal exponents Δ_q. Our numerical results are in agreement with analytical findings obtained using the sigma-model field theory.

Model. We use the model of Ref. [21]. The unitary part of the evolution is described by the nearest-neighbor tight-binding Hamiltonian $\hat{H} = -J\sum_{\langle \boldsymbol{x}\boldsymbol{x}'\rangle}[\hat{\psi}^{\dagger}_{\boldsymbol{x}}\hat{\psi}_{\boldsymbol{x}'} + \mathrm{H.c.}]$, defined on a d-dimensional cubic lattice with L^d sites and periodic boundary conditions. The nonunitary part consists of projective measurements of site occupancy numbers $\hat{n}_{\boldsymbol{x}} = \hat{\psi}^{\dagger}_{\boldsymbol{x}}\hat{\psi}_{\boldsymbol{x}}$ performed at each site at randomly and independently selected times with a rate γ, i.e., the probability for each site to be measured in a time interval dt is γdt. Each measurement induces a wave-function collapse to a state with $\hat{n}_{\boldsymbol{x}} = 0$ or 1, with the Born-rule probabilities. Since we explore physics at sufficiently large length scales, our results are generic, i.e., independent of microscopic details of the model; in particular, they also apply to models with weak monitoring. We focus on the $d = 2$ case. At the same time, to address the transition analytically, we utilize the ϵ expansion for $d = 1 + \epsilon$.

The system is prepared in an arbitrary pure Gaussian (Slater-determinant) state at half filling and is evolved for a sufficiently long time $T \to +\infty$ in order to reach a steady-state measure, which is independent of the initial state [20,21]. The final state is completely determined by a quantum trajectory, which includes positions, times, and outcomes of all measurements. Throughout the evolution, the Gaussian property of the state is preserved, allowing its complete and efficient description via the correlation matrix $\mathcal{G}_{\boldsymbol{x}\boldsymbol{x}'} \equiv \langle \hat{\psi}^{\dagger}_{\boldsymbol{x}}\hat{\psi}_{\boldsymbol{x}'}\rangle$, where angular brackets denote the quantum-mechanical average.

The key indicator of the MIPT in a charge-conserving free-fermion model is the particle-number covariance [21], defined for two separated regions A and B as

$$G_{AB} \equiv \langle \hat{N}_A\rangle\langle \hat{N}_B\rangle - \langle \hat{N}_A\hat{N}_B\rangle = \sum_{\boldsymbol{x}\in A}\sum_{\boldsymbol{x}'\in B}\mathcal{C}_{\boldsymbol{x}\boldsymbol{x}'}, \tag{1}$$

where $\mathcal{C}_{\boldsymbol{x}\boldsymbol{x}'}$ is the density correlation function,

$$\mathcal{C}_{\boldsymbol{x}\boldsymbol{x}'} \equiv \langle \hat{n}_{\boldsymbol{x}}\rangle\langle \hat{n}_{\boldsymbol{x}'}\rangle - \langle \hat{n}_{\boldsymbol{x}}\hat{n}_{\boldsymbol{x}'}\rangle = |\mathcal{G}_{\boldsymbol{x}\boldsymbol{x}'}|^2 - \mathcal{G}_{\boldsymbol{x}\boldsymbol{x}}\delta_{\boldsymbol{x}\boldsymbol{x}'}. \tag{2}$$

We note that the mutual information $\mathcal{I}(A:B)$, which is another observable commonly used to characterize MIPTs, is related to G_{AB} via $\mathcal{I}(A:B) \approx (2\pi^2/3)\,G_{AB}$. Here, the sign $\approx$ indicates that an exact formula [33] valid for any Gaussian state contains additional terms proportional to higher-order charge correlators. However, these terms are parametrically suppressed for $\gamma \ll J$ and, moreover, are numerically small [20] for any relation between γ and J, so that this relation holds with very good accuracy.

We consider a setup in which the linear sizes of regions A and B and the separation between them are of the order of the system size, $\ell_A, \ell_B, \ell_{AB} \sim L$. The averaged G_{AB} is then a useful quantity to determine the position of the transition, in view of its distinct thermodynamic-limit behavior in the two phases and at criticality [21],

$$\overline{G_{AB}} \sim \begin{cases} gL^{d-1}, & \text{diffusive,} \\ G_c = \mathrm{const}, & \text{critical,} \\ \exp\left(-\ell_{AB}/\ell_{\mathrm{loc}}\right), & \text{localized,} \end{cases} \tag{3}$$

with the effective diffuson constant $g = J/(2\sqrt{2}\gamma)$. Here, the overbar denotes the averaging over quantum trajectories, and ℓ_{loc} is the localization length. This behavior is directly related [see Eq. (1)] to the scaling of the average density correlation function:

$$\overline{\mathcal{C}_{\boldsymbol{x}\boldsymbol{x}'}} \sim \begin{cases} g|\boldsymbol{x}-\boldsymbol{x}'|^{-(d+1)}, & \text{diffusive,} \\ G_c|\boldsymbol{x}-\boldsymbol{x}'|^{-2d}, & \text{critical,} \\ \exp\left(-|\boldsymbol{x}-\boldsymbol{x}'|/\ell_{\mathrm{loc}}\right), & \text{localized.} \end{cases} \tag{4}$$

In Ref. [21], we focused on averaged observables, demonstrated the MIPT, and determined the critical measurement rate $\gamma_c/J \approx 2.93$ for this model by using Eq. (3). Now, we turn to the analysis of mesoscopic fluctuations over the ensemble of quantum trajectories. Below, we set $J = 1$, so that the control parameter γ/J becomes simply γ.

Numerical results. We performed simulations of the stochastic monitored evolution of a $d = 2$ free-fermion system of size $L \times L$ with periodic boundary conditions. The numerical analysis was carried out via direct exact evaluation of the full correlation matrix $\mathcal{G}_{\boldsymbol{x}\boldsymbol{x}'}$. To explore the scale dependence of observables, the system size L was varied between $L = 12$ and $L = 44$ in steps of 4. To gather sufficient statistics, we have sampled 1000 individual trajectory realizations for each system size. In addition, we have utilized spatial averaging over different positions in the system to further increase the statistical ensemble. For each individual quantum trajectory, we have extracted the distribution function of the particle-number covariance (1) for regions A and B of size $L/4 \times L$ separated by distance $L/4$, and of the density correlation function (2) at maximally separated points $\mathcal{C}_L \equiv \mathcal{C}_{\boldsymbol{x}\boldsymbol{x}'}$ with $\boldsymbol{x} - \boldsymbol{x}' = (L/2, L/2)$. Simulations were performed at the critical point, $\gamma = 2.93$, and in both diffusive ($\gamma = 0.5$ and 1.5) and localized ($\gamma = 4.5$) phases. Further details of simulations can be found in the Supplemental Material (SM) [34].

We begin with our analysis of the diffusive phase. Figure 1(a) shows the L dependence of the distribution function of the particle-number covariance. The distribution $P(G_{AB})$ is a nearly perfect Gaussian, down to the smallest system size. Furthermore, the width of this distribution, shown on Fig. 1(b), is size independent, $\mathrm{var}(G_{AB}) \approx 8.64 \times 10^{-3}$. These results are in agreement with the analytical predictions of "universal conductance fluctuations" (see SM [34]). (Similar behavior is also observed in the diffusive regime for $d = 1$.) At the same time, our numerical results for $\mathrm{var}(G_{AB})$ exhibit noticeable dependence on γ [34], at variance with the analytical prediction. Note that, while $\mathrm{var}(G_{AB})$ is independent of L, it does depend on the chosen geometry of regions A and B.

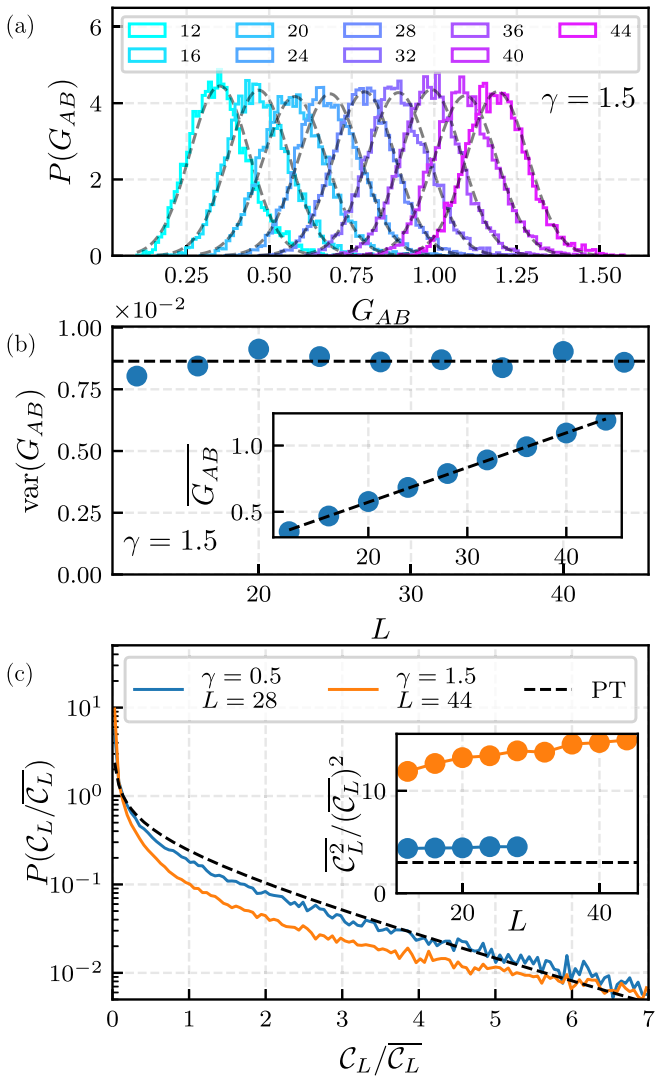

FIG. 1. Statistical properties of the diffusive phase. (a) Distribution of G_{AB} for $\gamma = 1.5$. Different colors correspond to different L (see legend). The distribution is nearly a perfect Gaussian, as demonstrated by Gaussian fits (dashed lines). (b) System size (in)dependence of variance of G_{AB}, demonstrating universal conductance fluctuations with fitted value (dashed line) $\mathrm{var}(G_{AB}) = 8.64 \times 10^{-3}$. Inset: size dependence of average $\overline{G_{AB}}$; dashed line: linear fit $G = (2.61L + 4.94) \times 10^{-2}$, consistent with the large-L scaling (3). (c) Distribution $P(z = \mathcal{C}_L/\overline{\mathcal{C}_L})$ of the density correlation function $\mathcal{C}_L$ normalized to its average for $\gamma = 1.5$ and 0.5; dashed line: Porter-Thomas (PT) distribution predicted analytically for $\gamma \ll 1$. Inset: L dependence of the second moment $\overline{z^2}$; dashed line: the analytical prediction $\overline{z^2} = 3$ for $\gamma \ll 1$.

In Fig. 1(c), we show the distribution function $P(z = \mathcal{C}_L/\overline{\mathcal{C}_L})$ of the density correlation function $\mathcal{C}_L$ normalized to its average value $\overline{\mathcal{C}_L}$ for two values of γ in the diffusive phase, $\gamma = 1.5$ and 0.5. The distribution $P(z)$ and its moments $\overline{z^q}$ are L independent (for L larger than the correlation length ℓ_{corr}), as illustrated in the inset for $q = 2$. Furthermore, when γ is reduced, the distribution approaches the limiting form $P(z) = e^{-z/2}/\sqrt{2\pi z}$ (known as Porter-Thomas distribution in a different context), with $\overline{z^q} = (2q-1)!!$, in agreement with our analytical result (see SM [34]). In the opposite case, when

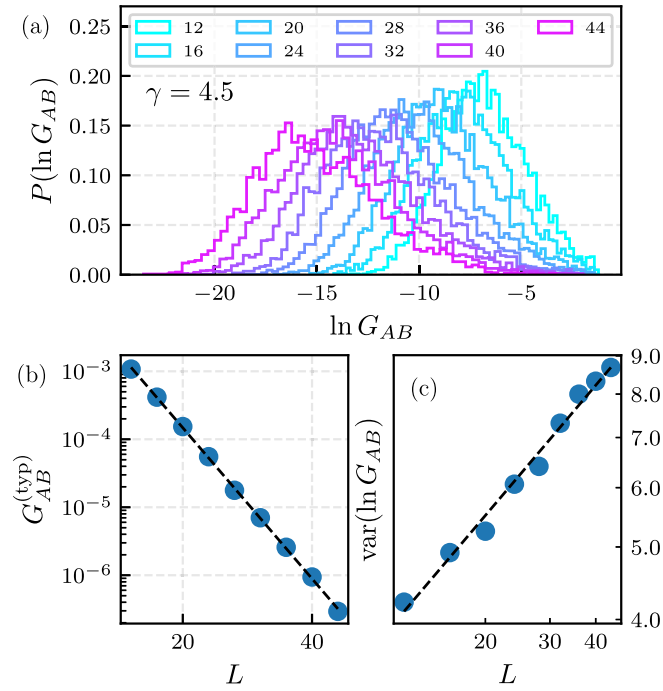

FIG. 2. Statistics of G_{AB} in the localized phase, $\gamma = 4.5$. (a) Distribution function of the *logarithm* of G_{AB}. Different colors correspond to different system sizes L (see legend). (b) L dependence of *typical* covariance $G_{AB}^{(\mathrm{typ})}$; dashed line: exponential fit $G_{AB}^{(\mathrm{typ})} \sim \exp(-L/4\ell_{\mathrm{loc}}^{(\mathrm{typ})})$ with $\ell_{\mathrm{loc}}^{(\mathrm{typ})} \approx 0.98$. (c) L dependence of the variance of $\ln G_{AB}$; dashed line: power-law fit $\mathrm{var}(\ln G_{AB}) \sim L^{\mu}$ with $\mu \approx 0.58$.

γ approaches the transition point, the moments $\overline{z^q}$ diverge $\sim \ell_{\mathrm{corr}}^{q-\Delta_q}$ due to multifractality at scales shorter than ℓ_{corr} (see below the results for the multifractal spectrum Δ_q characterizing the critical point). The strong enhancement of $\overline{z^2}$ for $\gamma = 1.5$ in comparison with its value $\overline{z^2} = 3$ at $\gamma \ll 1$ seen in inset of Fig. 1(c) is a manifestation of this behavior.

We now turn our attention to the other side of the transition and discuss the behavior in the localized phase. In Fig. 2(a), we show the distribution of the *logarithm* of the covariance G_{AB}. It is seen from Fig. 2(b) that the center of the distribution moves linearly with L in the negative direction, which corresponds to the typical value scaling as $G_{AB}^{(\mathrm{typ})} = \exp(\overline{\ln G_{AB}}) \sim \exp(-L/4\ell_{\mathrm{loc}}^{(\mathrm{typ})})$, i.e., to exponential localization. Further, we observe that the distribution broadens with increasing L, which is quantified in Fig. 2(c), where the variance of the distribution is shown as a function of L. The data clearly indicate a power-law scaling $\mathrm{var}(\ln G_{AB}) \propto L^{\mu}$ with an exponent $\mu \approx 0.58$. We find a similar behavior for the distribution of $\ln \mathcal{C}_{xx'}$ (see SM [34]), with a somewhat different numerical value of the exponent characterizing the scaling of the variance, $\mu \approx 0.43$. Asymptotically (at $L \to \infty$), the exponent μ should be the same for both observables, so that the apparent difference can be attributed to subleading (finite-size) corrections. This yields an estimate for the accuracy of the exponent, $\mu \approx 0.5 \pm 0.1$. The behavior that we find for the localized phase of the measurement problem is similar to that for the $D = d + 1 = 3$ Anderson-localization problem that

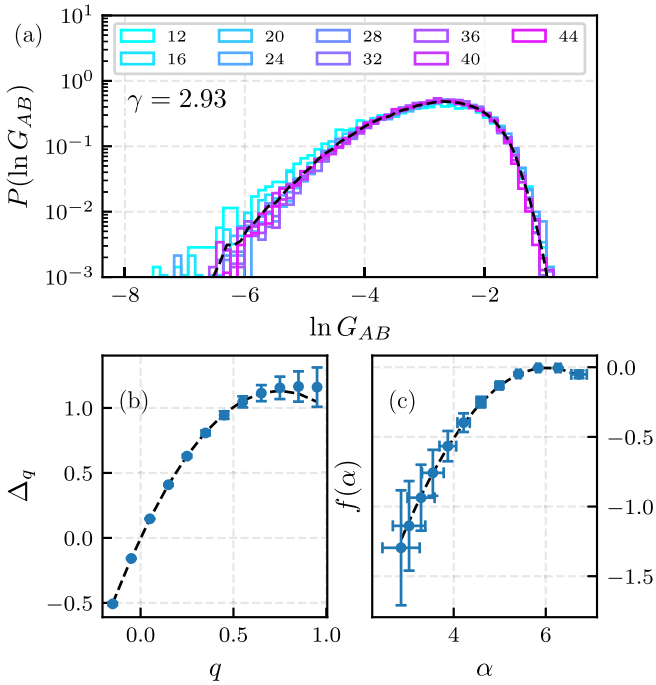

FIG. 3. Properties of the critical point, $\gamma = 2.93$. (a) Scale-invariant distribution function of $\ln G_{AB}$. Different colors correspond to different system sizes L (see legend). (b) Anomalous dimensions Δ_q of moments of the density correlation function $\mathcal{C}_{xx'}$. The Dashed line is the best parabolic fit according to $\Delta_q = q + cq(1-q)$, with $c \approx 2.04$. (c) Spectrum of multifractal dimensions $f(\alpha)$. Dashed line: parabolic fit according to $f(\alpha) = -[\alpha - (4+c)]^2/4c$, with $c \approx 2.03$.

was shown to be related to the directed-polymer and Kardar-Parisi-Zhang (KPZ) problems in $2+1$ dimensions (see SM [34] for a summary of key results with references). It remains to be seen whether there is exact correspondence between the corresponding exponents. It is plausible (although remains to be proven) that our exponent μ is equal to $\mu = 2\delta \approx 0.48$ where δ is the KPZ growth exponent in $2+1$ dimensions.

Finally, we analyze properties of systems at criticality, $\gamma \approx 2.93$. In Fig. 3(a), we present the distribution function $P(\ln G_{AB})$. It is seen to be L independent, in agreement with the expected scale invariance of the critical point. In Figs. 3(b) and 3(c), we demonstrate another manifestation of criticality: the multifractal statistics of the correlation function $\mathcal{C}_{xx'}$, which obeys the scaling $\overline{\mathcal{C}_L^q} \sim L^{-q(d+1)-\Delta_q}$. Here, the first term $-q(d+1)$ in the exponent corresponds to the diffusive scaling, while Δ_q is the anomalous dimension. The resulting exponents Δ_q are shown in Fig. 3(b) (see SM [34] for details of the fitting procedure and comparison with previous discussions of multifractality at MIPTs). The nonlinear dependence of Δ_q on q is a manifestation of multifractality.

We note that the *average* correlation function $\overline{\mathcal{C}_{xx'}}$ (corresponding to $q = 1$) is a correlation function of conserved currents and thus should follow at criticality the scaling [21] $\overline{\mathcal{C}_{xx'}} \sim |\boldsymbol{x} - \boldsymbol{x}'|^{-2d}$, implying $\Delta_1 = d - 1 = 1$, in good agreement with the numerical data. We further observe that the multifractality spectrum Δ_q is well approximated by the parabolic formula $\Delta_q = q + cq(1-q)$ shown by the dashed line in Fig. 3(b). This formula corresponds to a one-loop approximation [34], which is parametrically justified for a transition in $d = 1 + \epsilon$ dimensions with $\epsilon \ll 1$ (when the critical conductance is large) [35]. Note that, while the parabolic approximation is found to hold with good accuracy also for $d = 2$, it is only an approximation in view of higher-loop contributions to Δ_q.

An alternative (but equivalent) way to present the results on multifractality is as follows. For each value of the correlation function, we introduce the exponent $\alpha = -\ln \mathcal{C}_{xx'}/\ln|\boldsymbol{x} - \boldsymbol{x}'|$. This quantity itself is random, and its distribution function acquires the form $P(\alpha) \sim L^{f(\alpha)}$, where $f(\alpha)$ is termed the singularity spectrum. It is then easy to show that $f(\alpha)$ is related to anomalous dimensions via the Legendre transformation:

$$f(\alpha) = q\Delta_q' - \Delta_q, \quad \alpha = \Delta_q' + (d+1). \tag{5}$$

The obtained function $f(\alpha)$ is shown in Fig. 3(c). The position of its maximum, $\alpha_0 \approx 6$, determines the decay of the *typical* correlation function, $\mathcal{C}_{xx'}^{(\mathrm{typ})} \sim |\boldsymbol{x} - \boldsymbol{x}'|^{-\alpha_0}$, which is considerably faster than the decay of the average, $\overline{\mathcal{C}_{xx'}} \sim |\boldsymbol{x} - \boldsymbol{x}'|^{-4}$.

Summary and discussion. In this Letter, we have performed the analysis of mesoscopic fluctuations and multifractality across the MIPT in a monitored free-fermion system. Our numerical results for a $d = 2$ model are in full consistency with analytical predictions. Our findings for the statistics of the particle-number covariance G_{AB} and of the correlation function $\mathcal{C}(r)$ exhibit remarkable analogies with the mesoscopic physics of Anderson localization in disordered systems, with G_{AB} and $\mathcal{C}(r)$ being the counterparts of the two-terminal and two-point conductances, respectively. Within this analogy, G_{AB} and $\mathcal{C}(r)$ are governed by diffusive trajectories in $(d+1)$-dimensional space-time, which describe building and propagation of entanglement and particle-number correlations. The trajectories are formed by measurement events (serving essentially as "impurities" in space-time), with ballistic propagation between them.

On the delocalized side (measurement rate $\gamma < \gamma_c$), we demonstrate the "universal conductance fluctuations" of G_{AB} [Figs. 1(a) and 1(b)]. The moments of $\mathcal{C}(r)$ show a "diffusive" scaling, $\overline{\mathcal{C}^q}(r) \propto r^{-q(d+1)}$, with the distribution of $\mathcal{C}(r)/\overline{\mathcal{C}}(r)$ approaching the Porter-Thomas form for small γ and manifesting multifractality at scales shorter than the correlation length when γ increases towards the critical value γ_c. The Porter-Thomas form corresponds to Gaussian fluctuations of the correlation function $\mathcal{G}_{xx'}$, resulting, at small γ, from a sum of many individual-trajectory contributions. The universal conductance fluctuations of G_{AB} are governed by events of crossing for pairs of trajectories (as shown more formally in SM [34]). The probability of crossing of three or more trajectories is small for small γ, explaining the Gaussian form of the distribution of G_{AB}.

With increasing γ, the crossings of diffusive trajectories proliferate, leading to the development of localization and to dramatic enhancement of mesoscopic fluctuations. In the localized phase ($\gamma > \gamma_c$), we find a very broad distribution of G_{AB}, with $\overline{-\ln G_{AB}} \sim L$ and the variance $\mathrm{var}(\ln G_{AB}) \sim L^{\mu}$ (Fig. 2), and similarly for $\mathcal{C}(r)$, with $\mu \approx 0.5$. It is plausible that, for both quantities, μ is given asymptotically by the KPZ theory in $2+1$ dimensions, which implies $\mu \approx 0.48$. At

criticality ($\gamma = \gamma_c$), G_{AB} develops a scale-invariant distribution and $\mathcal{C}(r)$ exhibits multifractality (Fig. 3). The corresponding spectrum of multifractal anomalous dimensions is well approximated by the parabolic (one-loop) form $\Delta_q = q + cq(1-q)$ with $c \approx 2$.

Concerning the link to the Anderson-localization problem in $d+1$ dimensions, it is worth emphasizing the following. First, the formulation of the measurement problem is very different from that of Anderson localization, and the connection made evident via the nonlinear sigma model field theory, with the emergent isotropy of space-time, is rather nontrivial and remarkable. Second, there are important distinctions: the sigma model of the measurement problem is characterized by chiral symmetry, unconventional $R \to 1$ replica limit, absorbing condition at the boundary of the $d+1$-dimensional system corresponding to the time at which the observables are studied and unconventional geometry of the "terminals" (in terminology of the transport problems) A and B that both belong to this boundary. These differences essentially affect many of key properties, including, in particular, the power laws in Eq. (4), the multifractal spectrum Δ_q of the correlation function and its distribution in the diffusive phase, the shape of the distribution of G_{AB} at criticality, as well as the numerical value of the variance of its "universal" fluctuations in the diffusive phase.

Our work, which largely lays the foundations of mesoscopic physics of monitored systems, paves a way for various extensions. This includes investigation of systems of various dimensionalities, as well as symmetry and topology classes. In connection with the above comments, it will be very interesting to make a quantitative comparison with corresponding observables in the Anderson-localization problem. Another interesting question is the effect of interaction on mesoscopic fluctuations and multifractality.

Acknowledgments. We thank I. Gruzberg and P. Ostrovsky for useful discussions and acknowledge support by the Deutsche Forschungsgemeinschaft (DFG, German Research Foundation)–553096561.

Data availability. The data that support the findings of this article are openly available [36].

[1] Y. Li, X. Chen, and M. P. A. Fisher, Quantum Zeno effect and the many-body entanglement transition, Phys. Rev. B **98**, 205136 (2018).

[2] B. Skinner, J. Ruhman, and A. Nahum, Measurement-induced phase transitions in the dynamics of entanglement, Phys. Rev. X **9**, 031009 (2019).

[3] A. Chan, R. M. Nandkishore, M. Pretko, and G. Smith, Unitary-projective entanglement dynamics, Phys. Rev. B **99**, 224307 (2019).

[4] X. Cao, A. Tilloy, and A. De Luca, Entanglement in a fermion chain under continuous monitoring, SciPost Phys. **7**, 024 (2019).

[5] M. Szyniszewski, A. Romito, and H. Schomerus, Entanglement transition from variable-strength weak measurements, Phys. Rev. B **100**, 064204 (2019).

[6] Y. Li, X. Chen, and M. P. A. Fisher, Measurement-driven entanglement transition in hybrid quantum circuits, Phys. Rev. B **100**, 134306 (2019).

[7] Y. Bao, S. Choi, and E. Altman, Theory of the phase transition in random unitary circuits with measurements, Phys. Rev. B **101**, 104301 (2020).

[8] A. C. Potter and R. Vasseur, Entanglement dynamics in hybrid quantum circuits, in *Entanglement in Spin Chains: From Theory to Quantum Technology Applications*, edited by A. Bayat, S. Bose, and H. Johannesson (Springer, Cham, 2022), pp. 211–249.

[9] M. P. Fisher, V. Khemani, A. Nahum, and S. Vijay, Random quantum circuits, Annu. Rev. Condens. Matter Phys. **14**, 335 (2023).

[10] C. Noel, P. Niroula, D. Zhu, A. Risinger, L. Egan, D. Biswas, M. Cetina, A. V. Gorshkov, M. J. Gullans, D. A. Huse, and C. Monroe, Measurement-induced quantum phases realized in a trapped-ion quantum computer, Nat. Phys. **18**, 760 (2022).

[11] J. M. Koh, S.-N. Sun, M. Motta, and A. J. Minnich, Measurement-induced entanglement phase transition on a superconducting quantum processor with mid-circuit readout, Nat. Phys. **19**, 1314 (2023).

[12] J. C. Hoke, *et al.* (Google Quantum AI and Collaborators), Measurement-induced entanglement and teleportation on a noisy quantum processor, Nature (London) **622**, 481 (2023).

[13] U. Agrawal, J. Lopez-Piqueres, R. Vasseur, S. Gopalakrishnan, and A. C. Potter, Observing quantum measurement collapse as a learnability phase transition, Phys. Rev. X **14**, 041012 (2024).

[14] X. Turkeshi, A. Biella, R. Fazio, M. Dalmonte, and M. Schirò, Measurement-induced entanglement transitions in the quantum Ising chain: From infinite to zero clicks, Phys. Rev. B **103**, 224210 (2021).

[15] O. Alberton, M. Buchhold, and S. Diehl, Entanglement transition in a monitored free-fermion chain: From extended criticality to area law, Phys. Rev. Lett. **126**, 170602 (2021).

[16] M. Buchhold, Y. Minoguchi, A. Altland, and S. Diehl, Effective theory for the measurement-induced phase transition of Dirac fermions, Phys. Rev. X **11**, 041004 (2021).

[17] M. Coppola, E. Tirrito, D. Karevski, and M. Collura, Growth of entanglement entropy under local projective measurements, Phys. Rev. B **105**, 094303 (2022).

[18] F. Carollo and V. Alba, Entangled multiplets and spreading of quantum correlations in a continuously monitored tight-binding chain, Phys. Rev. B **106**, L220304 (2022).

[19] M. Szyniszewski, O. Lunt, and A. Pal, Disordered monitored free fermions, Phys. Rev. B **108**, 165126 (2023).

[20] I. Poboiko, P. Pöpperl, I. V. Gornyi, and A. D. Mirlin, Theory of free fermions under random projective measurements, Phys. Rev. X **13**, 041046 (2023).

[21] I. Poboiko, I. V. Gornyi, and A. D. Mirlin, Measurement-induced phase transition for free fermions above one dimension, Phys. Rev. Lett. **132**, 110403 (2024).

[22] K. Chahine and M. Buchhold, Entanglement phases, localization, and multifractality of monitored free fermions in two dimensions, Phys. Rev. B **110**, 054313 (2024).

[23] L. Lumia, E. Tirrito, R. Fazio, and M. Collura, Measurement-induced transitions beyond gaussianity: A single particle description, Phys. Rev. Res. **6**, 023176 (2024).

[24] E. Starchl, M. H. Fischer, and L. M. Sieberer, Generalized Zeno effect and entanglement dynamics induced by fermion counting, PRX Quantum **6**, 030302 (2025).

[25] M. Fava, L. Piroli, D. Bernard, and A. Nahum, Monitored fermions with conserved U(1) charge, Phys. Rev. Res. **6**, 043246 (2024).

[26] A. Zabalo, M. J. Gullans, J. H. Wilson, R. Vasseur, A. W. W. Ludwig, S. Gopalakrishnan, D. A. Huse, and J. H. Pixley, Operator scaling dimensions and multifractality at measurement-induced transitions, Phys. Rev. Lett. **128**, 050602 (2022).

[27] C.-M. Jian, H. Shapourian, B. Bauer, and A. W. W. Ludwig, Measurement-induced entanglement transitions in quantum circuits of non-interacting fermions: Born-rule versus forced measurements, arXiv:2302.09094.

[28] E. V. H. Doggen, Y. Gefen, I. V. Gornyi, A. D. Mirlin, and D. G. Polyakov, Evolution of many-body systems under ancilla quantum measurements, Phys. Rev. B **107**, 214203 (2023).

[29] Y. Le Gal, X. Turkeshi, and M. Schirò, Entanglement dynamics in monitored systems and the role of quantum jumps, PRX Quantum **5**, 030329 (2024).

[30] P. Pöpperl, I. V. Gornyi, D. B. Saakian, and O. M. Yevtushenko, Localization, fractality, and ergodicity in a monitored qubit, Phys. Rev. Res. **6**, 013313 (2024).

[31] B. Fan, C. Yin, and A. M. García-García, How does the entanglement entropy of a many-body quantum system change after a single measurement? arXiv:2504.04071.

[32] M. Pütz, R. Vasseur, A. W. W. Ludwig, S. Trebst, and G.-Y. Zhu, Flow to Nishimori universality in weakly monitored quantum circuits with qubit loss, arXiv:2505.22720.

[33] I. Klich and L. Levitov, Quantum noise as an entanglement meter, Phys. Rev. Lett. **102**, 100502 (2009).

[34] See Supplemental Material at http://link.aps.org/supplemental/10.1103/2k3q-h6lz for details of the theoretical analysis and computational approach, which includes Refs. [37–60].

[35] The ϵ expansion in one loop yields the parabolic formula $\Delta_q = \epsilon q + \epsilon q(1-q)$, which for $\epsilon = 1$ yields $c = 1$. This value is substantially smaller than $c \approx 2$ observed numerically, which is not unexpected since ϵ expansion is parametrically justified only for $\epsilon \ll 1$.

[36] I. Poboiko, I. V. Gornyi, and A. D. Mirlin, Data for "mesoscopic fluctuations and multifractality at and across measurement-induced phase transitions" [Dataset], Zenodo, 2025, http://doi.org/10.5281/zenodo.17722972.

[37] B. L. Al'tshuler, Fluctuations in the extrinsic conductivity of disordered conductors, Pis'ma Zh. Eksp. Teor. Fiz. **41**, 530 (1985) [JETP Lett. **41**, 648 (1985)].

[38] E. Bettelheim, I. A. Gruzberg, and A. W. W. Ludwig, Quantum Hall transitions: An exact theory based on conformal restriction, Phys. Rev. B **86**, 165324 (2012).

[39] B. M. Forrest and L.-H. Tang, Surface roughening in a hypercube-stacking model, Phys. Rev. Lett. **64**, 1405 (1990).

[40] C. L. Kane, R. A. Serota, and P. A. Lee, Long-range correlations in disordered metals, Phys. Rev. B **37**, 6701 (1988).

[41] J. Kelling and G. Ódor, Extremely large-scale simulation of a Kardar-Parisi-Zhang model using graphics cards, Phys. Rev. E **84**, 061150 (2011).

[42] E. Kogan, M. Kaveh, R. Baumgartner, and R. Berkovits, Statistics of waves propagating in a random medium, Phys. Rev. B **48**, 9404 (1993).

[43] E. Kogan and M. Kaveh, Random-matrix-theory approach to the intensity distributions of waves propagating in a random medium, Phys. Rev. B **52**, R3813 (1995).

[44] P. A. Lee, A. D. Stone, and H. Fukuyama, Universal conductance fluctuations in metals: Effects of finite temperature, interactions, and magnetic field, Phys. Rev. B **35**, 1039 (1987).

[45] P. A. Lee and A. D. Stone, Universal conductance fluctuations in metals, Phys. Rev. Lett. **55**, 1622 (1985).

[46] G. Lemarié, Glassy properties of Anderson localization: Pinning, avalanches, and chaos, Phys. Rev. Lett. **122**, 030401 (2019).

[47] E. Medina and M. Kardar, Quantum interference effects for strongly localized electrons, Phys. Rev. B **46**, 9984 (1992).

[48] A. D. Mirlin, R. Pnini, and B. Shapiro, Intensity distribution for waves in disordered media: Deviations from Rayleigh statistics, Phys. Rev. E **57**, R6285 (1998).

[49] C. Monthus and T. Garel, Random transverse field Ising model in dimension $d > 1$: Scaling analysis in the disordered phase from the directed polymer model, J. Phys. A: Math. Theor. **45**, 095002 (2012).

[50] S. Mu, J. Gong, and G. Lemarié, Kardar-Parisi-Zhang physics in the density fluctuations of localized two-dimensional wave packets, Phys. Rev. Lett. **132**, 046301 (2024).

[51] T. M. Nieuwenhuizen and M. C. W. van Rossum, Intensity distributions of waves transmitted through a multiple scattering medium, Phys. Rev. Lett. **74**, 2674 (1995).

[52] F. Pietracaprina, V. Ros, and A. Scardicchio, Forward approximation as a mean-field approximation for the anderson and many-body localization transitions, Phys. Rev. B **93**, 054201 (2016).

[53] J. Prior, A. M. Somoza, and M. Ortuño, Conductance fluctuations and single-parameter scaling in two-dimensional disordered systems, Phys. Rev. B **72**, 024206 (2005).

[54] B. Shapiro, Large intensity fluctuations for wave propagation in random media, Phys. Rev. Lett. **57**, 2168 (1986).

[55] A. M. Somoza, J. Prior, and M. Ortuño, Conductance fluctuations in the localized regime: Numerical study in disordered noninteracting systems, Phys. Rev. B **73**, 184201 (2006).

[56] A. M. Somoza, M. Ortuño, and J. Prior, Universal distribution functions in two-dimensional localized systems, Phys. Rev. Lett. **99**, 116602 (2007).

[57] D. Politis, J. Romano, and M. Wolf, *Subsampling*, Springer Series in Statistics (Springer, New York, 1999).

[58] A. D. Mirlin, Statistics of energy levels and eigenfunctions in disordered systems, Phys. Rep. **326**, 259 (2000).

[59] N. Swain, S. Adam, and G. Lemarié, 2D anderson localization and KPZ sub-universality classes: Sensitivity to boundary conditions and insensitivity to symmetry classes, arXiv:2504.17010.

[60] S. A. van Langen, P. W. Brouwer, and C. W. J. Beenakker, Nonperturbative calculation of the probability distribution of plane-wave transmission through a disordered waveguide, Phys. Rev. E **53**, R1344 (1996).